# Thickness-dependent mechanical failure in thin films of glassy polymer bidisperse blends

*Tianren Zhang,*[†] *Robert A. Riggleman*[*, †]

†Department of Chemical and Biomolecular Engineering, University of Pennsylvania, Philadelphia, Pennsylvania 19104, United States

**ABSTRACT.** Although many studies have analyzed the various properties of glassy polymer thin films, the failure mode and nonlinear mechanical response has only recently received attention. Due to competing effects between reductions in the entanglement density and increased mobility near the free surfaces, it is not clear whether one should anticipate embrittlement or improved ductility. In this study, we constructed polymer thin films with a bidisperse molecular weight distribution by incorporating short chains as diluents into highly entangled polymer systems at different compositions and film thickness. Due to the dominance of the high-mobility region near the free surfaces, films approximately 10 monomer diameters thick are less ductile than thicker films comprised of either a bidisperse blend or a homopolymer, despite having a similar entanglement density. The dependence of mechanical properties on the thickness is weak when the film is larger than $20\sigma$, especially for highly entangled systems. With diluent polymers added, the films become less ductile, and the mechanical properties of the polymer thin films are affected most when the added diluents are unentangled polymers, as expected. Further, we observe a competing effect between free surface and entanglement network, where the free surface

interaction dominates the mechanical behavior for the thinnest films tested while the entanglement network plays a dominant role in thicker films.

## Introduction

As nanotechnology becomes increasingly pervasive, polymers are of critical importance for a wide variety of thin film applications such as next-generation lithography, lubricating coatings, and sensors. Many studies have investigated the thickness dependence of glass transition temperature[1–6], $T_g$, segmental relaxations[7–11], entanglement network[12–16], and chain conformations[17–19] in polymer films. In addition to the large changes in $T_g$ in free-standing thin films due to the enhanced mobility near free surfaces, the mechanical properties of polymer films are also altered compared to the bulk. These changes are both due to the surface interactions at the interface of thin films and reduction in the entanglement density; however, nonlinear mechanical properties, including failure, have only recently been studied.

There are numerous techniques to probe the elastic properties of polymer films. Indirect measurement methods, such as thin film buckling [20,21], and Brillouin light scatter (BLS) [22,23], have been used to investigate the elastic and tensile responses of the thin film at different thickness. While most studies conclude that the elastic constants of thin films deviate from bulk as the film thickness decreases below 30-40nm[20,24,25], though there are notable exceptions that remain unresolved[26]. Recently, Crosby and coworkers directly measured the complete uniaxial stress-strain response, including failure, for films as thin as 10nm by floating the polystyrene (PS) films on liquid substrates. Their experiments demonstrated that the modulus and failure stress for PS films decreases as the film thickness decreases below the average configuration size of chains, $R_{ee}$[27]. Notably, they provided the first visualization of a thickness-dependent failure mode, where

crazing was observed in thicker films and shear deformation zones (SDZ) in the thinnest films[28]. While these initial films floating on water, more recently Bay et al. characterized the complete stress-strain response of free-standing films as thin as 30 nm using a custom-built uniaxial tensile tester. They identified that liquid substrates enhance craze stability for PS films compared to freestanding films[29]. More surprisingly, ductile behaviors relative to the bulk were observed for free-standing PS films with the thicknesses ranging from $200nm - 500nm$. However, the enhanced ductility in those free standing films has not been fully understood, and the films were still relatively thick[30] compared to those where changes in $T_g$ are observed.

Molecular dynamic (MD) simulations have previously been applied to explore the elastic properties of ultrathin films, and several studies examined the molecular details of elastic behavior and plastic flow in polymer films[31]. Van Workum and de Pablo explored the size dependence on the apparent modulus of nanostructures by imposing deflection or compressive deformations on nanoscale beams fixed on a substrate using both continuum mechanics and molecular simulations[32]. They observed that the bending modulus of the glassy nanostructure remains bulk like until the width approaches $20\sigma$, where $\sigma \approx 1$ nm for polystyrene (PS) or poly(methyl methacrylate) (PMMA). Similarly, systematically-derived coarse-grained simulations of PS and PMMA showed that the elastic moduli are reduced at a thickness of 40 nm compared to the bulk, and the size of softer layer at the free surface is only a few nanometers[33]. By applying high-frequency sinusoidal oscillations on the free-standing films, Yoshimoto et al. also found that a mechanically soft layer is present near the free surface [34] in the dynamic mechanical properties of coarse-grained polymers.

Separately, the entanglement network in high molecular weight polymers is also critical in determining the mechanical properties, which could lead to ductility during tensile extension and cause craze formation[35]. Experimentally, Wang et al. investigated the load-bearing strands (LBSs) between the junctions in the affinely strained chain network during deformation for glassy polymers. The authors argue that for temperatures above the brittle-to-ductile transition (BDT), the polymer chain tension builds up in LBSs and activates adjacent LBSs sequentially, which drives yielding and plastic flow. In their work, they noted that the density of LBS is proportional to the chain thickness and flexibility but may be distinct from the entanglement network[36]. Molecular modeling studies have also examined failure and craze formation in bulk polymer glasses. Baljon and Robbins showed that when the length of polymer chain is less than number of monomers between entanglements, $N_e$, the film breaks along a simple fracture plane; however, crazing occurs at a constant plateau stress when the length of chain is greater than $N_e$, before the samples break[37].

Blending chemically identical unentangled and entangled polymers is a practical means to systematically tune the density of entanglements and examine their effect on the dynamics and mechanics of a polymer. By blending a high molecular weight polystyrene (PS) with unentangled PS, the mixture will exhibit a brittle to ductile transition, and the network of long chains enables plastic flow during the uniaxial compression[38]. In addition, the high molecular weight component was found to strongly influence the craze initiation stress due to the increase in entanglement density[39]. While several studies have been performed in bulk bidisperse blends of chemically identical polymers, understanding how distributions of the lengths of chains in polymer blends affect mechanical properties is still relatively unexplored in thin films where the chain conformations and entanglement density can be perturbed away from bulk.

In this study, we use MD simulations to investigate the nonlinear mechanical properties of glassy, free-standing polymer films of bidisperse model polymers as a function of the bidisperse blend molecular weight and volume fraction. We constructed several bidisperse systems by blending highly entangled polymers with low molecular-weight diluents where the low molecular weight additive spans from unentangled to weakly entangled, and the film thickness varied from highly confined to bulk-like. By examining the uniaxial stress-strain response, strain localization during deformation, and entanglements of those systems, we show how the entanglement network of different blend compositions affect the mechanical behaviors of ultrathin films. Competing effects from the free surface and the entanglement network modulate the behavior at different film thicknesses.

**Model and methods**

Our molecular dynamics simulations employed a modified version of the bead−spring Kremer−Grest (KG) model[40], where non-bonded interactions among monomers are taken through the Lennard-Jones (LJ) potential,

$$U_{ij}^{nb} = 4\varepsilon\left[\left(\frac{\sigma}{r}\right)^{12} - \left(\frac{\sigma}{r}\right)^{6}\right] - 4\varepsilon\left[\left(\frac{\sigma}{r_{cut}}\right)^{12} - \left(\frac{\sigma}{r_{cut}}\right)^{6}\right], \quad (1)$$

for $r \leq r_{cut} = 2.5\sigma$. All the units are made dimensionless using the potential strength, $\varepsilon$, the monomer size, $\sigma$, and the unit time $\tau = \sigma(m/\varepsilon)^{\frac{1}{2}}$, where $m$ is the monomer mass. The bonded interactions between two connected monomers are governed by a finitely extensible nonlinear elastic (FENE) potential with $k = 30\varepsilon/\sigma^2$ and $R_0 = 1.5\sigma$. This bond type does not allow bond breaking during the uniaxial deformation process. We additionally add an angular harmonic potential

$$U_{ang} = \frac{K_\theta}{2}(\theta - \theta_0)^2, \quad (2)$$

where $K_\theta = 10\varepsilon/radian^2$ is the strength of this interaction and $\theta_0 = 120^o$ is the equilibrium bond angle. The angular potential is introduced to increase the average number of entanglements per chain without having very long polymer chain lengths, and the resulting average number of monomers between the entanglements is $\langle N_e \rangle \approx 16$. The number of monomers per chain in our simulations are $N = 10$, 30, 60, or 250, with $N/N_e = 0, 1.8, 3.75$ and $15.9$ respectively. Bidisperse polymer blends are constructed by incorporating the shorter chains ($N = 10, 30,$ or 60), which are treated as diluents, into the $N = 250$ systems at different film thickness ($H = 10\sigma, 20\sigma$ and $30\sigma$). The composition details of the long chains and short chains at various film thickness are shown in supporting Table S1.

Free standing polymer films were created by randomly growing polymers inside a rectangular box with a surface area of $\sim 3R_{ee,N=250} \times 3R_{ee,N=250}$, where $R_{ee,N=250}$ is the equilibrium end-to-end distance of $N = 250$, and the box height depends on the target film thickness. Periodic boundary conditions were maintained in the plane of the film ($x$ and $y$-directions), and initially we employed reflective walls on the top and bottom edge of the box in the z direction. The density of monomer beads was initially set to $\rho_s = 0.85/\sigma^{-3}$ inside the simulation box. After placing the polymers in the box, we first used a soft potential to eliminate overlapping contacts[41] before switching to the standard LJ potential. After $\tau$=100 of MD at $T = 1.0$, we turned off the reflective walls and also enlarged the box both directions along the z direction so that the height of the box is approximately twice the target thickness of the films to realize a free-standing film. Next, connectivity-altering Monte Carlo moves[41–43] were employed to accelerate the equilibration of the thin film systems. The equilibration proceeded until we observed diffusive behavior of the center of mass mean-

squared displacement (MSD), which is calculated with a moving time origin to improve the statistics. Three independent configurations of the films for each system were generated at high temperatures, and we then cooled those polymer films from $T = 1.0$ ($\frac{T}{T_{g,bulk}} = 1.67$) to $T = 0.4$ ($\frac{T}{T_{g,bulk}} = 0.67$) with a cooling rate of $\Delta T/\Delta t$ = 0.1 per $2000\tau$ to generate our glassy polymer thin films. Subsequently, we uniaxially deformed each film under a constant temperature at a constant true rate $\dot{\varepsilon} = 1 \times 10^{-4}$ in the x direction. Due to the extended simulation box in the $z$-direction, the samples are effectively at constant pressure and can change volume during deformation by contracting in the $z$-direction. All the simulations are performed using LAMMPS MD simulation package[44] with the velocity Verlet algorithm under an NVT ensemble.

To study strain localization, the deviatoric strain rate $J_2$ for each particle is calculated during the deformation as[45–48]

$$J_{2,i}(\varepsilon, \varepsilon + \Delta\varepsilon) = \frac{1}{\Delta\varepsilon}\sqrt{\frac{1}{3}Tr[\boldsymbol{\eta}_i - \eta_i^m \boldsymbol{I}]^2}\,. \tag{3}$$

Here $\boldsymbol{\eta}_i = \frac{1}{3}(\boldsymbol{J}_i^T \boldsymbol{J}_i - \boldsymbol{I})$ is the strain tensor for particle $i$, $\boldsymbol{J}_i$ is the best affine transformation matrix[49] calculated based on the neighboring particles within distance of $2.5\sigma$ for particle $i$ at strain $\varepsilon$ over a certain lag strain $\Delta\varepsilon$, and $\boldsymbol{I}$ is the identity matrix. A high $J_{2,i}$ value implies a high shear strain rate for particle $i$.

To identify strain localization homogeneous plastic flow, we apply a metric that was established in our previous work to define the mesoscale character of the strain response[50]. In this calculation, the spatial variations of average $J_2$ between pairs of slabs are calculated by dividing the thin films into 12 equal-thickness slabs along the deformation direction. We defined this quantity as $S_L$ by taking average over all pairs of slabs,

$$S_L(T,\varepsilon;\varepsilon_w)=\frac{1}{n_b(n_b-1)}\sum_{i=1}^{n_b}\sum_{j=1,j\neq i}^{n_b}\langle\left(\overline{J_2(i,\varepsilon)}-\langle\overline{J_2(j)}\rangle_{\varepsilon_w}\right)^2\rangle_{\varepsilon_w} \quad (4)$$

$$\cdot\langle\left(\overline{J_2(j,\varepsilon)}-\langle\overline{J_2(i)}\rangle_{\varepsilon_w}\right)^2\rangle_{\varepsilon_w}$$

where $n_b$ is the number of blocks, the overhead bar is the average of $J_2$ over all particles inside the block, and $\varepsilon_w$ denotes the strain window where the $J_2$ values are calculated. In this calculation, we let $\varepsilon_w$ to be the same as the value of lag strain used in calculations of $J_2$, $\Delta\varepsilon$ = 4%. More detailed information about this calculation is provided in our previous study [50]. This metric can give us a good understand of the spatial inhomogeneity of the strain during deformation process.

## Results and discussion

### 3.1 Local relaxation

Due to the presence of the free surfaces in the free-standing films, the segmental dynamics throughout the films are affected as the films thickness decreases. To better understand the free surface induced confinement effect, the local relaxation time of monomers $\tau_\alpha(z)$ based on the positions along the height of the films at $\frac{T}{T_{g,bulk}}=1.05$ are calculated. The changes in the

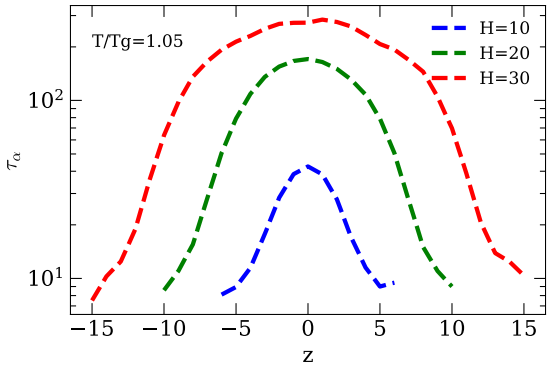


**Figure 1.** The local relaxation time of monomers $\tau_\alpha(z)$ as a function of position along the height of the thin films in homopolymer thin film N=250 at temperature $\frac{T}{T_{g,bulk}}=1.05$.

relaxation time at this temperature extend over 10 monomer diameters away from the interface and the largest observed changes are a factor of approximately 30 increase in the mobility at the surface of the films compared to the center. As shown in Fig. 1, the relaxation time in the center of the $H = 10\sigma$ films are approximately 7 times smaller than that for the $H = 30\sigma$ films. Below we will argue that the significant enhancement in mobility in the thinnest films is the origin of the reduced toughness in these films.

### 3.2 **Entanglement analysis**

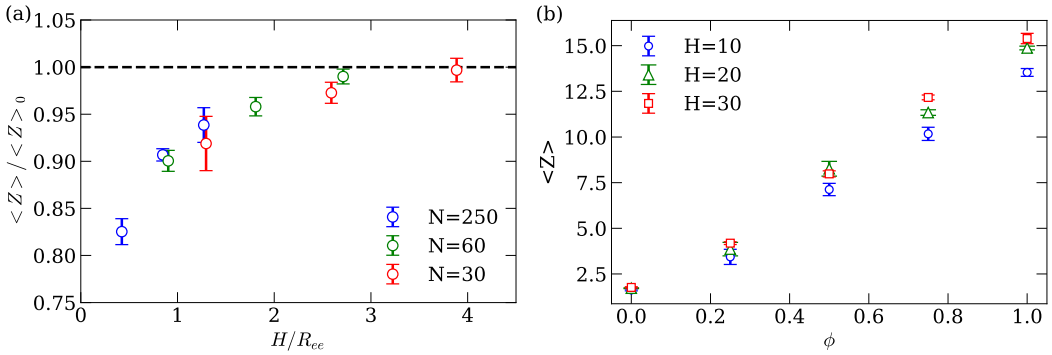


**Figure 2**. (a) Normalized average entanglement per chain of the homopolymer thin films as a function of the degree of confinement $\frac{H}{R_{ee}}$. (b) Average entanglements per chain $\langle Z \rangle$ only for the polymer with chain length of $N = 250$ as a function of $\phi$ in the binary blend polymer thin films at different thickness and the polymer diluent chain length is $N = 30$. $\phi$ is the monomer-based percentage of $N = 250$ in the mixture.

To determine the average number of entanglements per chain $\langle Z \rangle$ in the bidisperse blend systems, the Z1 algorithm is applied to extract the mean number of interior kinks per chain by straightening the polymer chains without allowing them to cross each other, and at the end the polymers are reduced into lines connected through "kinks" where the chains bend around neighboring chains.

This estimate for $\langle Z \rangle$ is proportional to the number of entanglements, regardless of the details of the definition used to define an entanglement from topological data[51]. The properties of the entanglement network were extracted for all films far above $T_{g,bulk}$ at $T = 1.0$. As expected from previous work[13], in the homopolymer films $\langle Z \rangle$ is reduced as the film thickness $H/R_{ee}$ decreases, as shown in Fig. 2a. The maximum reduction observed in this work for the most confined systems (where $\frac{H}{R_{ee}} = 0.26$) is nearly $20\%$. Further, we applied the entanglement analysis in the bidisperse blend polymer mixtures to extract the average number of entanglements per chain $\langle Z \rangle$ where we only count those entanglements between the polymer chains with length of $N = 250$; the low molecular weight diluents are removed from the configuration before performing the analysis. As we show below, the low molecular weight polymers ($N = 30$ in this case) are unable to support mechanical load even though $\langle Z \rangle > 1$, consistent with prior work[52,53]. In Figure 2b we observe a linear correlation between composition of long chains and $\langle Z \rangle$ across all the film thickness, which is consistent with entanglement studies for bulk bidisperse blends[54]. We also notice a similar trend between fraction of long chains and $\langle Z \rangle$ if we take all the polymers into account for the entanglement analysis, as shown in the supporting information (Fig. S1).

### 3.3 **Mechanical response**

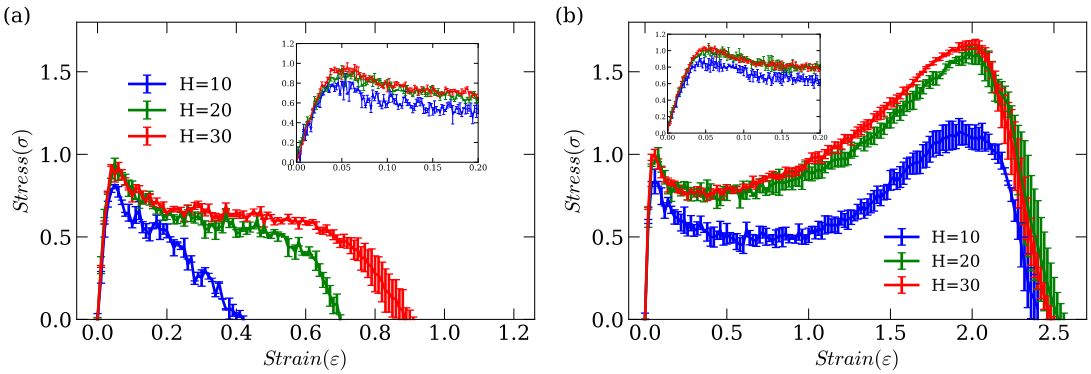


**Figure 3**. Uniaxial deformation true stress-strain responses of homopolymer thin films $N = 30$ (a) and $N = 250$ (b) at temperature $\frac{T}{T_{g,bulk}} = 0.71$. The embedding small plots are the stress-strain responses at early strains.

We begin our study of the mechanics by comparing the mechanical response of unblended homopolymer films as a function of film thickness. For slightly entangled homopolymer chains N $= 30$ and with a film thickness above $20\sigma$, in Fig 3a we observe an initial elastic regime, yielding and strain softening, and a plastic plateau until the chain pullout causes failure of the films. However, for our thinnest films with $H = 10\sigma$, after the yield point, we observed a different failure mechanism where the stress decreases more rapidly with strain, and the plastic plateau regime almost disappears. A similar stress-strain behavior exhibits for the system with longer diluents of $N = 60$, and the results are shown in the supporting information (Fig.S2). For highly entangled films with $N = 250$, in the plastic plateau craze widening is evident, as discussed below. Moreover, we observe pronounced strain hardening after the plastic plateau across all film thicknesses before failure. These regimes are qualitatively consistent with crazing behaviors in the bulk[53], albeit differences are expected given the simulations are carried out for thin films. The mechanical

response of the $H = 10\sigma$ film undergoes a more pronounced strain softening, and the plastic plateau exists at a lower stress level, as shown in Fig. 3b. The differences of stress-strain responses between film with $H = 20\sigma$ and $H = 30\sigma$ include a slightly delayed onset in strain hardening and smaller maximum in the stress before failure in the $H = 20\sigma$ film.

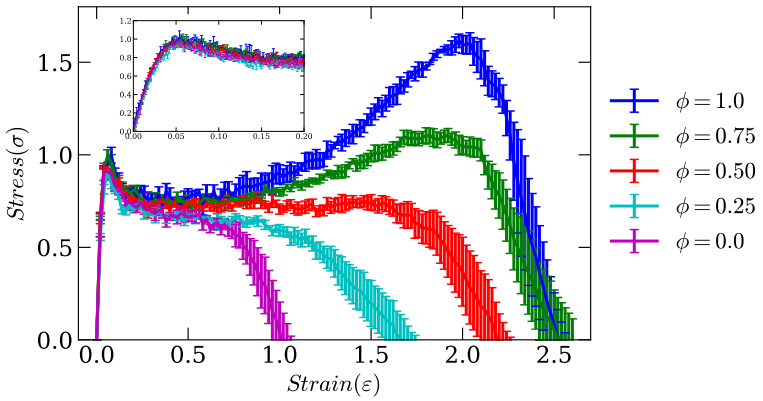


**Figure 4**. Uniaxial deformation stress-strain response of blended thin films with mixture of $N = 250$ and $N = 60$ at temperature $\frac{T}{T_{g,bulk}} = 0.71$ and film thickness $H = 20\sigma$. $\phi$ corresponds to the monomer-based percentage of $N = 250$ in the mixture, and the insets highlight the early strain response.

Next, we investigate the mechanical responses for bidisperse blended polymer films to analyze the composition-dependent mechanical properties. In Fig.4 we plot the stress-strain responses for a single film thickness $H = 20\sigma$ for different compositions of the long chains $N = 250$ versus diluents of $N = 60$. As the percentage of the $N = 250$ chains increase, the plastic plateau is extended, and at the highest concentrations strain hardening emerges. Similar behaviors are also observed for the mixture with diluents of $N = 30$ (supporting Fig.S3). We have also analyzed the thickness effect on the bidisperse blends where analogous trends are observed for homopolymer thin films where the $H = 10\sigma$ films are softer and fail at smaller strains (supporting Fig.S4). In

the bulk, Hoy and Robbins found the "stress superposition principle", where $\sigma_{blend} = \phi\sigma_{long} + (1-\phi)\sigma_{short}$, in blend polymers under moderate strain.[55] Similar results are also observed in the thick films ($H = 20\sigma$ and $H = 30\sigma$) at strain $\varepsilon < 0.5$ and $\phi > 0.5$. However, in the films $H = 10\sigma$, the results deviate from stress superposition since the free surface also plays an important role in determining the stress in the ultrathin films in addition to chain entanglement and chain orientation.

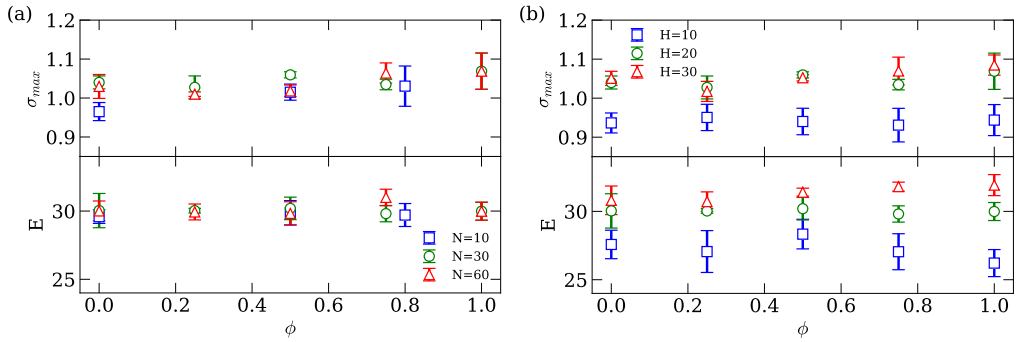


**Figure 5**. First maximum stress and elastic modulus as a function of (a) percentage of chain $N = 250$: with different diluents ($N = 10, 30, 60$ respectively) at film thickness $H = 20\sigma$ and (b) film thickness $H = 10, 20, 30\sigma$ with fixed diluents chain length $N = 30$.

To summarize the mechanical properties for this series of films, we measured elastic modulus $E$ and the strength $\sigma_{max}$ , taken as the first maximum of the stress. In Fig.5a, we observe that neither E nor $\sigma_{max}$ are dramatically affected by the diluent volume fraction nor the diluent chain length at fixed film thickness. In addition, we examined the thickness effect for those bidisperse blend polymers in Fig.5b with the chain length of the diluents fixed at $N = 30$. It shows that the thin films with $H = 10\sigma$ tend to have lower elastic modulus and lower yield stress than the two thicker films, while the same differences between film thickness at $H = 20\sigma$ and $H = 30\sigma$ are comparable to the sizes of our uncertainties. These results on the thickness dependence of the

mechanical properties of thin films are qualitatively consistent with the findings for the polystyrene thin films floating on water substrates[27,28].

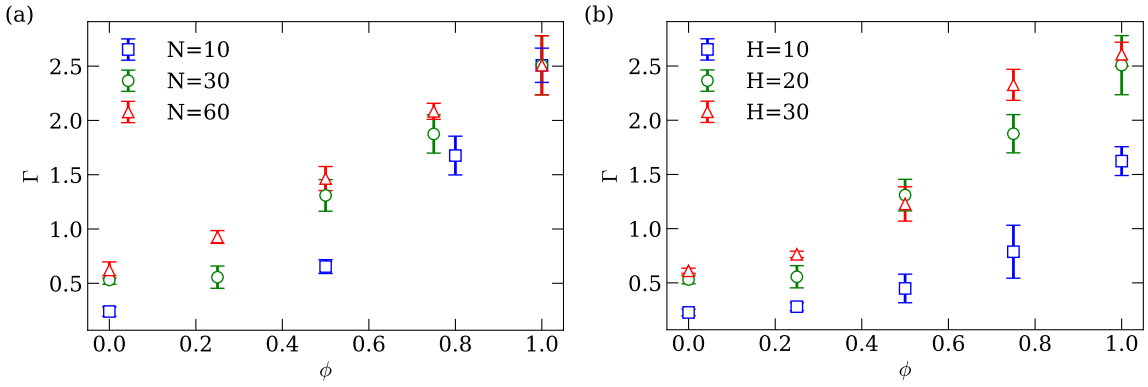


**Figure 6**. Bidisperse blend thin film toughness as a function of percentage of chain $N = 250$ with different diluents ($N = 10, 30, 60$ respectively) at film thickness $H = 20\sigma$ (a), with fixed diluents chain length $N = 30$ at different film thickness $H = 10, 20, 30\sigma$ respectively (b).

We quantify the toughness of the bidisperse blend polymer and homopolymer thin films by integrating the stress-strain response, $\Gamma = \int_0^{\varepsilon_{\sigma=0}} \sigma(\varepsilon) d\varepsilon$, where $\varepsilon_{\sigma=0}$ denotes the $\varepsilon$ value at which $\sigma(\varepsilon)$ crosses zero. As shown in Fig.6a for films with thickness of $H = 20\sigma$, the toughness of the thin films monotonically increases with the percentage increase of the $N = 250$ chains in the mixtures across all diluent chain lengths. For the unentangled diluent polymers $N = 10$, the toughness of the thin film increases slowly for $\phi < 0.5$, then more rapidly as $\phi$ approaches 1. At the value of $\phi = 0.5$, the toughness in systems with $N = 10$ diluents is approximately 50% that of the systems with $N = 30$ or $N = 60$ diluents. Further, systems with the $N = 60$ diluents are only slightly tougher than those with chain length of $N = 30$ at low $\phi$ ($\phi \leq 0.25$). The effect of film thickness on the toughness of the films is summarized in Fig.6b, where we observe that polymer thin film with thickness below $10\sigma$ have a notably reduced toughness compared to the thicker films across all the blend compositions, particularly at lower $\phi$. For films

with $H \geq 20\sigma$, the differences among the toughness at a given composition are negligible, which is consistent with the trends in the elastic modulus and maximum stress results above.

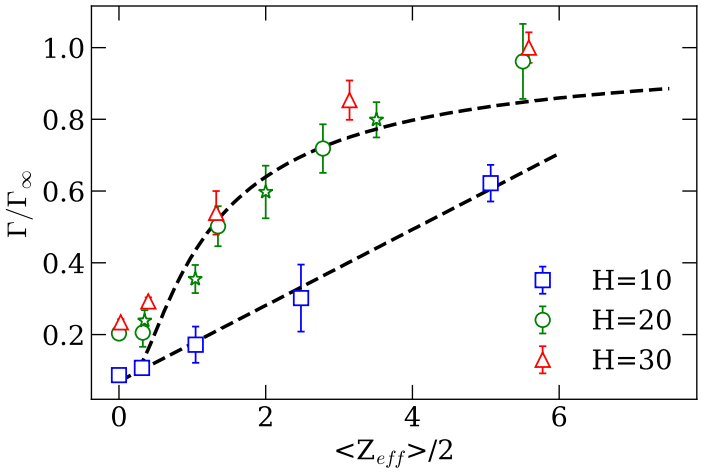


**Figure 7**. Toughness as a function of the average effective entanglements per $N = 250$ chain $\langle Z_{eff} \rangle$ in our bidisperse blends at three different film thicknesses. The different points for a given thickness correspond to different volume fractions of the short diluent chains. The star symbols represent the system with diluents of $N = 60$ at film thickness $H = 20\sigma$, while the other symbols involve only $N = 30$ diluents. $\Gamma_\infty$ is the toughness value of homopolymer systems $N = 250$ and $H = 30\sigma$. The top dashed line corresponds to the model proposed in our previous work, and the bottom dashed line is a linear fit to the $H = 10\sigma$ data. The data for $H = 20\sigma$ is extracted from our previous work.[56]

To further explore the relationship between entanglements the and mechanical properties of films, we applied the model developed from our previous work on bidisperse films[56]. The model is based on Mikos and Peppas's[57] theory, which we extended and showed that film toughness is exponentially proportional to the average number of mechanically effective entanglements per chain $\langle Z_{eff} \rangle$. The primitive path network of polymer chains is extracted via the Z1 algorithm[51]. The number of entanglements per chain is calculated by identifying "kinks" in the primitive path

network that is output from the Z1 code. At each entanglement location, four primitive path steps emanate around a central point corresponding to two primitive path steps on each chain. To calculate the number of mechanically effective entanglements, $\langle Z_{eff} \rangle$ we do not count any entanglements where any of the four primitive path steps involve a chain end. Importantly, this means that if an entanglement involves chains *i* and *j* and one of the primitive path steps on chain *i* involves a chain end, the entanglement does not count for either chain. In this calculation, all the polymer chains in the bidisperse blends are considered. As shown in Fig 7, the film thickness effect is essentially absent for both $H = 20\sigma$ and $30\sigma$, and the toughness can be described by the model from our previous work[56]. However, when the film thickness is $H = 10\sigma$, we find that the toughness exhibits a linear relationship with $\langle Z_{eff} \rangle$, which is what is expected in a polymer melt rather than a glass. The high mobility free surfaces dominate the mechanical behaviors of the films, despite having approximately the same density of entanglements in the systems. As shown above in the local relaxation time profiles, the overall relaxation time of the thinnest films $H = 10\sigma$ is much smaller compared to that of the two thicker films. Given the high portion of the free surfaces in the films, we surmise that the mechanical properties of the films are dominated by the fast dynamics of the monomers in the thinnest films.

### 3.3 **Failure morphology in thin films**

Fig. 8 shows snapshots of our films during deformation where each monomer is colored by the instantaneous $J_2$ calculated over a lag strain of 4%. The blue in the color scales represents particles that are not rearranging, and the red represents the $J_2$ value where around 99.9% of the particles have a smaller $J_2$ over the course of the entire trajectory. In Fig. 8, we compared homopolymers thin films between two different chain lengths at N=30 and N=250 at a film thickness $H = 10\sigma$,

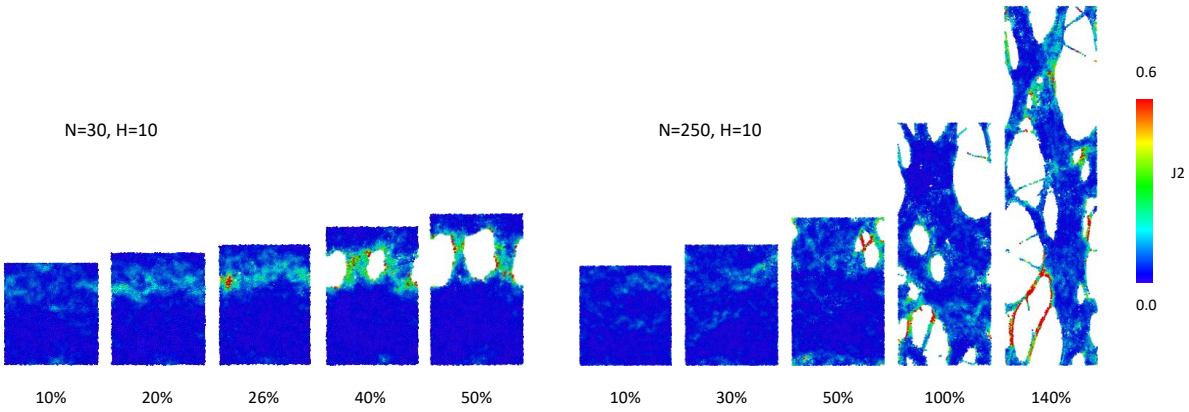


**Figure 8**. Snapshots of $N = 30$ homopolymer films (on the left), and N= 250 homopolymer films (on the right) with film thickness of $H = 10\sigma$ at different strains during deformation. The particles are color code by their $J_2$ value where the red corresponds to the $J_2$ value where around 99.9% of the particles have a smaller $J_2$ over the course of the entire trajectory.

and the same polymers with $H = 30\sigma$ are shown in Fig. S5. For N =30, the polymer systems are weakly entangled, and we observed a necking and a formation of plastic zone, where strain is highly localized. This qualitative observation is independent of film thickness, though the thick film sustains much larger strain before failure. In the snapshots for large strains and $N = 30$, only a small number of chains are drown into the plastic zone where failure occurs, as expected for chain length less than $2N_e$[37,58].

For thin films with highly entangled polymers, we observe a 2D craze structure for all film thicknesses; the entire region of the film is pulled into the plastic zone at larger strains before failure. We only observe 2D crazes for all film thicknesses, and we do not observe shear band formation, as observed from previous experimental studies where shear bands are present in polystyrene films thinner than 30 nm[28]. The differences between the observations from our simulation and the experiments may be rationalized since craze formation depends on the entanglement density and temperature[59,60], and our systems are more entangled than the

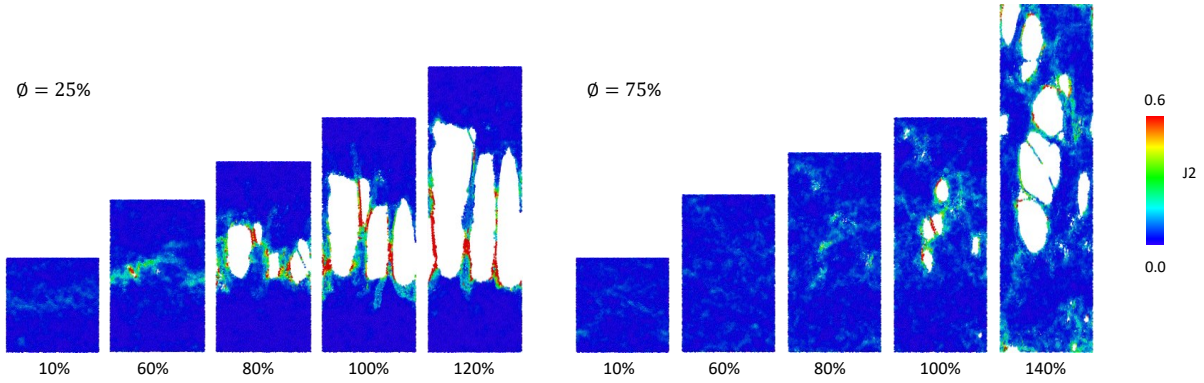


**Figure 9**. Snapshots of blend polymer films with diluent N= 30 at different percentage of N= 250 during deformation and the film thickness is hold at $H = 20\sigma$. The color scheme follows the same protocol as in Figure 8.

experiments [28]. In addition, we speculate that the monomeric friction of our coarse-grained models is significantly weaker than in experiments. To support this speculation, we note that at no point do we observe bonds stretched to the point where we might expect chain scission (at bond energies of $50 - 100\varepsilon$) as is believed to occur in experiments, though additional study would be necessary to quantify the friction for our model. A final possible distinction is the possibility of finite size effects in our simulations; the displacement of the edge of our simulation box to reach the yield point is comparable to the size of a molecule in our simulations, while experiments are orders of magnitude larger, and a more detailed discussion on this point can be found in our previous work[56]. By tuning the blend composition between the long chains $N = 250$ and short chains $N = 30$ of $H = 20\sigma$ films, we find that $\phi = 0.75$, almost all the polymers get drawn into the plastic zone and crazing takes place all over the film, as shown in Fig. 9. On the other hand, fewer polymers are drawn into plastic zone at high strains when $\phi = 0.5$ (supporting Fig. S6) and a clear blue region, where the chains are essentially immobile, is observed in the images. At the lowest nonzero $\phi =$

0.25, strain localization resembles that in the films with only short chains, where we observe a small plastic zone form at early strains where the film fails.

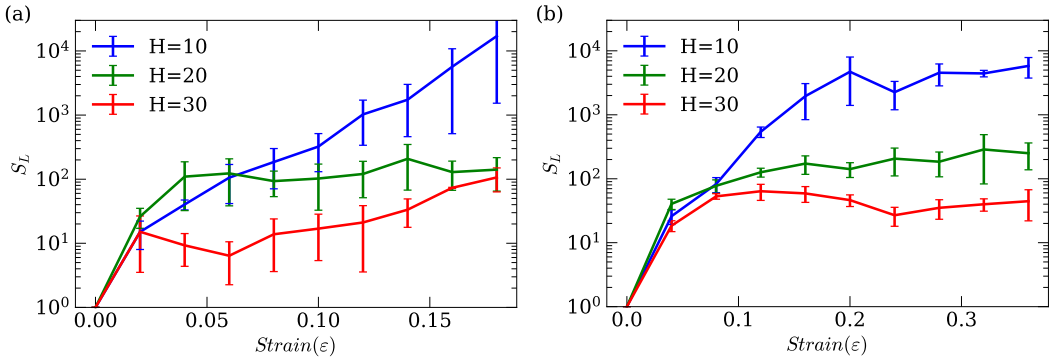


**Figure 10**. $S_L$ as a function of the total strain for homopolymer thin films with $N = 30$(a) and $N = 250$(b) respectively.

To understand the degree of strain localization, we examine the $S_L$ function defined above section for the films as a function of strain in Fig. 10. In both systems with $N = 30$ and $N = 250$, $S_L$ rises significantly with decreased thickness at a given strain. For thinnest films with $H = 10\sigma$, the magnitude of the spatial fluctuations in strain rate raises substantially as the strain increases, which indicates more pronounced strain localization. As the strain localization in the thicker films is not as strong as that in the $H = 10\sigma$ films, $S_L$ plateaus at a smaller value in the thick films. The significantly larger $S_L$ values observed in the thinnest films further supports that the mechanical behaviors observed in the thin films with thickness below $10\sigma$ are distinct from those of the thicker films.

## Conclusions

In summary, we have examined the thickness dependence of the mechanical behavior, including the stress-strain response, toughness, and failure mode in bidisperse blends of chemically identical model homopolymers using MD simulations. Due to the enhanced mobility of particles near the

free surface, the mechanical properties of our thinnest films with $H = 10\sigma$ are distinct from the thicker films, showing a reduced toughness compared to the thicker films analyzed. In these thinnest films, the entanglement network is only modestly affected by confinement, which leads to the conclusion that free surface effect dominates the mechanical behavior when the thickness of the polymer films is less than $10\sigma$ for this model system. When the film is $20\sigma$ or larger, changes in the mechanical response are minimal. During deformation, we observed plastic flow in all the polymeric systems, and all films exhibited a highly ductile response. The lack of brittle failure is hypothesized to be due to either the reduced monomeric friction in coarse-grained models or due to finite size effects in our simulations, as substantial finite size effects have been recently reported in simulations of silica glasses[61].

By tuning the volume fraction of high molecular weight polymers in bidisperse blend polymers systems, the mechanical properties of the thin films are altered, and we find that the toughness of the polymer thin film improves as the volume fraction of the low molecular weight diluents decreases for all the thin film thicknesses. The toughness changes more rapidly in films diluted with unentangled polymers. When holding the composition of the blend mixture constant, as the diluent polymer chain lengths increases the films become more ductile due to the increasing stability of the entanglement network in the systems. Using previously defined effective, or load-bearing entanglements and a modified[56] version of the Mikos and Peppas model[57], we found that when the film thickness is over $20\sigma$, the toughness of the films almost exhibits an exponential dependence on the average number of effective entanglements per chain. However, for the thin films with $\mathrm{H} = 10\sigma$, a linear relationship between toughness and effective entanglements is observed. To distinguish the free surface effect from entanglement effects, we calculated the local segmental relaxation in the polymer thin films, and found that for our thinnest films, there is a

large increase in the local dynamics across the entire film. This enhanced mobility dominates the properties during deformation and leads to a reduced toughness in the thin films.

In this work, we have focused solely on changes in the film thickness at a constant absolute temperature. Given the well-known tendency for confinement to freestanding films to lead to changes in $T_g$, some aspect of the changes in mechanical response with thickness could potentially be rationalized by simply choosing different temperatures for each film (e.g., at a constant $T/T_{g,bulk}$ or $T - T_{g,bulk}$). Given the broad distribution of relaxation times in the films[5,6,10,62], the lack of a "bulk-like" region for any of the films considered here, and the fact that the temperature dependence of mobility varies by location in the film[1,6,62,63], choosing an appropriate temperature scaling is nontrivial. This point will be carefully considered in a future study.

ASSOCIATED CONTENT

**Supporting Information**.

Supporting stress-strain responses of thin films, snapshots of the films labeled by deviatoric strain rate at different conditions (PDF).

AUTHOR INFORMATION

**Corresponding Author**

*E-mail rrig@seas.upenn.edu (R.A.R.).

**Author Contributions**

The manuscript was written through contributions of all authors. All authors have given approval to the final version of the manuscript.

**Funding Sources**

Z.T., and R.A.R. acknowledge support from NSF DMR 1904776. This research used the Extreme Science and Engineering Discovery Environment (XSEDE), which is supported by NSF ACI-1548562, accessed through allocation TG-DMR 150034.

ACKNOWLEDGMENT

The authors gratefully acknowledge funding support from the National Science Foundation through award NSF DMR-1904776 and computational resources provided by XSEDE allocation DMR-150034. The authors also thank Alfred J. Crosby, Konane Bay, and Cynthia Bukowski for helpful discussions.

REFERENCES

(1) Ediger, M. D.; Forrest, J. A. Dynamics near Free Surfaces and the Glass Transition in Thin Polymer Films: A View to the Future. *Macromolecules* **2014**, *47* (2), 471–478.
(2) Forrest, J. A.; Dalnoki-Veress, K.; Dutcher, J. R. Interface and Chain Confinement Effects on the Glass Transition Temperature of Thin Polymer Films. *Phys. Rev. E - Stat. Physics, Plasmas, Fluids, Relat. Interdiscip. Top.* **1997**, *56* (5), 5705–5716.
(3) Dalnoki-Veress, K.; Forrest, J. A.; Murray, C.; Gigault, C.; Dutcher, J. R. Molecular Weight Dependence of Reductions in the Glass Transition Temperature of Thin, Freely Standing Polymer Films. *Phys. Rev. E - Stat. Physics, Plasmas, Fluids, Relat. Interdiscip. Top.* **2001**, *63* (3), 1–10.
(4) Tsui, O. K. C.; Zhang, H. F. Effects of Chain Ends and Chain Entanglement on the Glass Transition Temperature of Polymer Thin Films. *Macromolecules* **2001**, *34* (26), 9139–9142.
(5) Varnik, F.; Baschnagel, J.; Binder, K. Reduction of the Glass Transition Temperature in Polymer Films: A Molecular-Dynamics Study. *Phys. Rev. E* **2002**, *65* (2), 021507.
(6) Paeng, K.; Ediger, M. D. Molecular Motion in Free-Standing Thin Films of Poly(Methyl Methacrylate), Poly(4-Tert-Butylstyrene), Poly(α-Methylstyrene), and Poly(2-Vinylpyridine). *Macromolecules* **2011**, *44* (17), 7034–7042.
(7) Yang, Z.; Fujii, Y.; Lee, F. K.; Lam, C.; Tsui, O. K. C. Glass Transition Dynamics And. *Science (80-. ).* **2010**, *328* (June), 1676–1679.
(8) Shavit, A.; Riggleman, R. A. Physical Aging, the Local Dynamics of Glass-Forming Polymers under Nanoscale Confinement. *J. Phys. Chem. B* **2014**, *118* (30), 9096–9103.
(9) Mirigian, S.; Schweizer, K. S. Theory of Activated Glassy Relaxation, Mobility Gradients, Surface Diffusion, and Vitrification in Free Standing Thin Films. *J. Chem. Phys.* **2015**, *143* (24).

(10) Shavit, A.; Riggleman, R. A. Influence of Backbone Rigidity on Nanoscale Confinement Effects in Model Glass-Forming Polymers. *Macromolecules* **2013**, *46* (12), 5044–5052.
(11) Hesami, M.; Steffen, W.; Butt, H. J.; Floudas, G.; Koynov, K. Molecular Probe Diffusion in Thin Polymer Films: Evidence for a Layer with Enhanced Mobility Far above the Glass Temperature. *ACS Macro Lett.* **2018**, *7* (4), 425–430.
(12) Si, L.; Massa, M. V; Dalnoki-Veress, K.; Brown, H. R.; Jones, R. A. L. Chain Entanglement in Thin Freestanding Polymer Films. *Phys. Rev. Lett.* **2005**, *94* (12), 127801.
(13) Sussman, D. M. Spatial Distribution of Entanglements in Thin Free-Standing Films. *Phys. Rev. E* **2016**, *94* (1), 012503.
(14) Sussman, D. M.; Tung, W.-S.; Winey, K. I.; Schweizer, K. S.; Riggleman, R. A. Entanglement Reduction and Anisotropic Chain and Primitive Path Conformations in Polymer Melts under Thin Film and Cylindrical Confinement. *Macromolecules* **2014**, *47* (18), 6462–6472.
(15) Meyer, H.; Kreer, T.; Cavallo, A.; Wittmer, J. P.; Baschnagel, J. On the Dynamics and Disentanglement in Thin and Two-Dimensional Polymer Films. *Eur. Phys. J. Spec. Top.* **2007**, *141* (1), 167–172.
(16) Pressly, J. F.; Riggleman, R. A.; Winey, K. I. Increased Polymer Diffusivity in Thin-Film Confinement. *Macromolecules* **2019**, *52* (16), 6116–6125.
(17) Behavior, T.; Cavallo, A.; Mu, M.; Binder, K. Unmixing of Polymer Blends Confined in Ultrathin Films : Crossover Between. **2005**, 6544–6552.
(18) Jones, R. L.; Kumar, S. K.; Ho, D. L.; Briber, R. M.; Russell, T. P. Chain Conformation in Ultrathin Polymer Films. *Nature* **1999**, *400* (6740), 146–149.
(19) Brûlet, A.; Boué, F.; Menelle, A.; Cotton, J. P. Conformation of Polystyrene Chain in Ultrathin Films Obtained by Spin Coating. *Macromolecules* **2000**, *33* (3), 997–1001.
(20) Torres, J. M.; Stafford, C. M.; Vogt, B. D. Elastic Modulus of Amorphous Polymer Thin Films: Relationship to the Glass Transition Temperature. *ACS Nano* **2009**, *3* (9), 2677–2685.
(21) Stafford, C. M.; Vogt, B. D.; Harrison, C.; Julthongpiput, D.; Huang, R. Elastic Moduli of Ultrathin Amorphous Polymer Films. *Macromolecules* **2006**, *39* (15), 5095–5099.
(22) Sun, L.; Dutcher, J. R.; Giovannini, L.; Nizzoli, F.; Stevens, J. R.; Ord, J. L. Elastic and Elasto-Optic Properties of Thin Films of Poly(Styrene) Spin Coated onto Si(001). *J. Appl. Phys.* **1994**, *75* (11), 7482–7488.
(23) Cheng, W.; Sainidou, R.; Burgardt, P.; Stefanou, N.; Kiyanova, A.; Efremov, M.; Fytas, G.; Nealey, P. F. Elastic Properties and Glass Transition of Supported Polymer Thin Films. *Macromolecules* **2007**, *40* (20), 7283–7290.
(24) Stafford, C. M.; Harrison, C.; Beers, K. L.; Karim, A.; Amis, E. J.; Vanlandingham, M. R.; Kim, H. C.; Volksen, W.; Miller, R. D.; Simonyi, E. E. A Buckling-Based Metrology for Measuring the Elastic Moduli of Polymeric Thin Films. *Nat. Mater.* **2004**, *3* (8), 545–550.
(25) Stafford, C. M.; Vogt, B. D.; Harrison, C.; Julthongpiput, D.; Huang, R. Elastic Moduli of Ultrathin Amorphous Polymer Films. *Macromolecules* **2006**, *39* (15), 5095–5099.
(26) O'Connell, P. A.; McKenna, G. B. Rheological Measurements of the Thermoviscoelastic Response of Ultrathin Polymer Films. *Science (80-. ).* **2005**, *307* (5716), 1760–1763.
(27) Liu, Y.; Chen, Y. C.; Hutchens, S.; Lawrence, J.; Emrick, T.; Crosby, A. J. Directly Measuring the Complete Stress-Strain Response of Ultrathin Polymer Films. *Macromolecules* **2015**, *48* (18), 6534–6540.
(28) Bay, R. K.; Shimomura, S.; Liu, Y.; Ilton, M.; Crosby, A. J. Confinement Effect on Strain

Localizations in Glassy Polymer Films. *Macromolecules* **2018**, *51* (10), 3647–3653.
(29) Bay, R. K.; Crosby, A. J. Uniaxial Extension of Ultrathin Freestanding Polymer Films. *ACS Macro Lett.* **2019**, *8* (9), 1080–1085.
(30) Velez, N. R.; Allen, F. I.; Jones, M. A.; Govindjee, S.; Meyers, G. F.; Minor, A. M. Extreme Ductility in Freestanding Polystyrene Thin Films. *Macromolecules* **2020**, *53* (19), 8650–8662.
(31) Yang, F.; Ghosh, S.; Lee, L. J. Molecular Dynamics Simulation Based Size and Rate Dependent Constitutive Model of Polystyrene Thin Films. *Comput. Mech.* **2012**, *50* (2), 169–184.
(32) Van Workum, K.; De Pablo, J. J. Computer Simulation of the Mechanical Properties of Amorphous Polymer Nanostructures. *Nano Lett.* **2003**, *3* (10), 1405–1410.
(33) Xia, W.; Lan, T. Interfacial Dynamics Governs the Mechanical Properties of Glassy Polymer Thin Films. *Macromolecules* **2019**, *52* (17), 6547–6554.
(34) Yoshimoto, K.; Jain, T. S.; Nealey, P. F.; De Pablo, J. J. Local Dynamic Mechanical Properties in Model Free-Standing Polymer Thin Films. *J. Chem. Phys.* **2005**, *122* (14), 1–6.
(35) Ge, T.; Tzoumanekas, C.; Anogiannakis, S. D.; Hoy, R. S.; Robbins, M. O. Entanglements in Glassy Polymer Crazing: Cross-Links or Tubes? *Macromolecules* **2017**, *50* (1), 459–471.
(36) Wang, S. Q.; Cheng, S.; Lin, P.; Li, X. A Phenomenological Molecular Model for Yielding and Brittle-Ductile Transition of Polymer Glasses. *J. Chem. Phys.* **2014**, *141* (9), 1–19.
(37) Baljon, A. R. C.; Robbins, M. O. Simulations of Crazing in Polymer Glasses: Effect of Chain Length and Surface Tension. *Macromolecules* **2001**, *34* (12), 4200–4209.
(38) Liu, J.; Lin, P.; Cheng, S.; Wang, W.; Mays, J. W.; Wang, S. Q. Polystyrene Glasses under Compression: Ductile and Brittle Responses. *ACS Macro Lett.* **2015**, *4* (10), 1072–1076.
(39) Sánchez-Valencia, A.; Smerdova, O.; Hutchings, L. R.; De Focatiis, D. S. A. The Roles of Blending and of Molecular Weight Distribution on Craze Initiation. *Macromolecules* **2017**, *50* (23), 9507–9514.
(40) Kremer, K.; Grest, G. S. Erratum: Dynamics of Entangled Polymer Melts: A Molecular-dynamics Simulation [J. Chem. Phys. 9 2 , 5057 (1990)]. *J. Chem. Phys.* **1991**, *94* (5), 4103–4103.
(41) Sides, S. W.; Grest, G. S.; Stevens, M. J.; Plimpton, S. J. Effect of End-Tethered Polymers on Surface Adhesion of Glassy Polymers. *J. Polym. Sci. Part B Polym. Phys.* **2004**, *42* (2), 199–208.
(42) Mavrantzas, V. G.; Boone, T. D.; Zervopoulou, E.; Theodorou, D. N. End-Bridging Monte Carlo: A Fast Algorithm for Atomistic Simulation of Condensed Phases of Long Polymer Chains. *Macromolecules* **1999**, *32* (15), 5072–5096.
(43) Banaszak, B. J.; De Pablo, J. J. A New Double-Rebridging Technique for Linear Polyethylene. *J. Chem. Phys.* **2003**, *119* (4), 2456–2462.
(44) Plimpton, S. Fast Parallel Algorithms for Short-Range Molecular Dynamics. *J. Comput. Phys.* **1995**, *117* (1), 1–19.
(45) Ivancic, R. J. S.; Riggleman, R. A. Identifying Structural Signatures of Shear Banding in Model Polymer Nanopillars. *Soft Matter* **2019**, *15* (22), 4548–4561.
(46) Adibi, S.; Branicio, P. S.; Liontas, R.; Chen, D. Z.; Greer, J. R.; Srolovitz, D. J.; Joshi, S. P. Surface Roughness Imparts Tensile Ductility to Nanoscale Metallic Glasses. *Extrem. Mech. Lett.* **2015**, *5*, 88–95.
(47) Li, W.; Rieser, J. M.; Liu, A. J.; Durian, D. J.; Li, J. Deformation-Driven Diffusion and

Plastic Flow in Amorphous Granular Pillars. *Phys. Rev. E - Stat. Nonlinear, Soft Matter Phys.* **2015**, *91* (6), 1–13.
(48) Shimizu, F.; Ogata, S.; Li, J. Theory of Shear Banding in Metallic Glasses and Molecular Dynamics Calculations. *Mater. Trans.* **2007**, *48* (11), 2923–2927.
(49) Falk, M. L.; Langer, J. S. Dynamics of Viscoplastic Deformation in Amorphous Solids. *Phys. Rev. E* **1998**, *57* (6), 7192–7205.
(50) Lin, E. Y.; Riggleman, R. A. Distinguishing Failure Modes in Oligomeric Polymer Nanopillars. *Soft Matter* **2019**, *15* (32), 6589–6595.
(51) Hoy, R. S.; Foteinopoulou, K.; Kröger, M. Topological Analysis of Polymeric Melts: Chain-Length Effects and Fast-Converging Estimators for Entanglement Length. *Phys. Rev. E* **2009**, *80* (3), 031803.
(52) Rottler, J.; Barsky, S.; Robbins, M. O. Cracks and Crazes: On Calculating the Macroscopic Fracture Energy of Glassy Polymers from Molecular Simulations. *Phys. Rev. Lett.* **2002**, *89* (14), 1–4.
(53) Rottler, J.; Robbins, M. O. Growth, Microstructure, and Failure of Crazes in Glassy Polymers. *Phys. Rev. E - Stat. Physics, Plasmas, Fluids, Relat. Interdiscip. Top.* **2003**, *68* (1), 18.
(54) Kramer, E. J.; Berger, L. L. Fundamental Processes of Craze Growth and Fracture BT - Crazing in Polymers Vol. 2; Kausch, H.-H., Ed.; Springer Berlin Heidelberg: Berlin, Heidelberg, 1990; pp 1–68.
(55) Hoy, R. S.; Robbins, M. O. Strain Hardening in Bidisperse Polymer Glasses: Separating the Roles of Chain Orientation and Interchain Entanglement. *J. Chem. Phys.* **2009**, *131* (24).
(56) Bukowski, C.; Zhang, T.; Riggleman, R. A.; Crosby, A. J. Load-Bearing Entanglements in Polymer Glasses. *Sci. Adv.* **2021**, *7* (38), 1–10.
(57) Mikos, A. G.; Peppas, N. A. Polymer Chain Entanglements and Brittle Fracture. *J. Chem. Phys.* **1988**, *88* (2), 1337–1342.
(58) Ethier, J. G.; Drummy, L. F.; Vaia, R. A.; Hall, L. M. Uniaxial Deformation and Crazing in Glassy Polymer-Grafted Nanoparticle Ultrathin Films. *ACS Nano* **2019**, *13* (11), 12816–12829.
(59) Kramer, E. J. Craze Fibril Formation and Breakdown. *Polym. Eng. Sci.* **1984**, *24* (10), 761–769.
(60) Berger, L. L.; Kramer, E. J. The Effect of Temperature on the Transition from Crazing to Shear Deformation in Crosslinked Polystyrene. *J. Mater. Sci.* **1988**, *23* (10), 3536–3543.
(61) Zhang, Z.; Ispas, S.; Kob, W. The Critical Role of the Interaction Potential and Simulation Protocol for the Structural and Mechanical Properties of Sodosilicate Glasses. *J. Non. Cryst. Solids* **2020**, *532* (December 2019), 119895.
(62) Diaz-Vela, D.; Hung, J. H.; Simmons, D. S. Temperature-Independent Rescaling of the Local Activation Barrier Drives Free Surface Nanoconfinement Effects on Segmental-Scale Translational Dynamics near Tg. *ACS Macro Lett.* **2018**, *7* (11), 1295–1301.
(63) Fakhraai, Z.; Forrest, J. A. Measuring the Surface Dynamics of Glassy Polymers. *Science (80-. ).* **2008**, *319* (5863), 600–604.